# Halide–Induced Cooperative Acid–Base Behavior at a Negatively Charged Interface

**ARTICLE** *in* THE JOURNAL OF PHYSICAL CHEMISTRY C · MARCH 2013

Impact Factor: 4.77 · DOI: 10.1021/jp401164r



**3 AUTHORS**, INCLUDING:

Md Shafiul Azam
Bangladesh University of Engineering and Tec…
**13** PUBLICATIONS **115** CITATIONS
SEE PROFILE

Julianne M Gibbs-Davis
University of Alberta
**37** PUBLICATIONS **748** CITATIONS
SEE PROFILE

THE JOURNAL OF PHYSICAL CHEMISTRY C

Article

pubs.acs.org/JPCC

# Halide-Induced Cooperative Acid–Base Behavior at a Negatively Charged Interface

Md. Shafiul Azam, Champika N. Weeraman, and Julianne M. Gibbs-Davis*

Department of Chemistry, University of Alberta, Edmonton, Alberta T6G 2G2, Canada

Supporting Information

**ABSTRACT:** Using second harmonic generation and sum frequency generation spectroscopy, we monitor the influence of sodium and potassium halides on acid–base processes at the negatively charged silica/aqueous electrolyte interface. We find that the two types of acidic silanols at the surface are very sensitive to the presence of halides in the aqueous phase. As the halide size increases, the pH at which half the more acidic sites are deprotonated ($pH_{0.5}$) shifts to lower pH. Conversely, the $pH_{0.5}$ of the less acidic sites shifts to higher pH with increasing halide size. We also observe titration curves of increasing sharpness as the halide size increases, indicative of positive cooperativity. Using a simple cooperative model, we find that the cooperative unit for the dissociation of more acidic surface sites is ~1, 2, and 3 for the chloride, bromide, and iodide electrolytes, respectively, which reveals that the larger anions promote deprotonation among the more acidic silanol groups. We also find that the fraction of more acidic sites, proportional to the relative surface charge density at neutral pH, increases from 20% to 86% as the sodium halide is varied from chloride to iodide. As the percentage of more acidic sites and the surface charge at neutral pH increases, the effective acidity of the less acidic sites decreases, indicating that greater surface charge density renders the remaining silanol groups more difficult to deprotonate. As the relative amount of less acidic sites increases, their deprotonation events exhibit negative, rather than positive, cooperativity revealing charge repulsion between neighboring silanol groups.

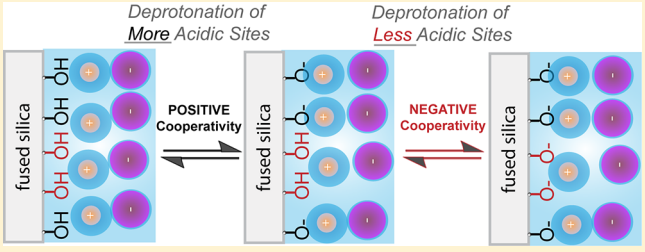


## 1. INTRODUCTION

The silica/water interface is involved in numerous geochemical, environmental, and industrial processes. Many of these processes such as pollutant transport and weathering involve the electrostatic interactions of aqueous species with the charged oxide surface and thus largely depend on the acid–base chemistry of the silica/water interface.[1−3] Consequently, there is a long history of research aimed at identifying the dissolution and acid–base chemistry of silica, particularly for colloidal and gel morphologies.[4−7]

One challenge in monitoring acid–base equilibria of silica particles is that the stability of colloidal dispersions is often pH dependent.[4] As a result, many potentiometric methods employed to monitor the change in particle mobility as a function of charge can only operate over a limited pH range, making it difficult to map out the entire acid–base equilibrium. One way to avoid aggregate instability is to study the macroscopic planar silica/water interface. Nonlinear optical methods like second harmonic generation and sum frequency generation can be utilized to monitor these buried interfaces based on the break in centrosymmetry that the interface presents.[8−12] For example, using vibrational sum frequency generation (SFG), the interfacial hydrogen-bonding network of water at the silica interface has been studied as a function of pH,[13−15] electrolyte concentration,[16,17] and electrolyte composition.[18] From the SFG spectra, Shen and co-workers concluded in the first investigation at this interface that two major populations of water were present: one weakly coordinated and the other strongly coordinated with respect to hydrogen bonds.[13] As the pH was made more basic, the relative distribution of these two populations varied significantly. Second harmonic generation (SHG), a related nonlinear optical technique, has been used as a complementary method to probe changes in the potential of the interface. Monitoring the SHG signal as a function of pH indicated that the planar silica/water interface possessed two unique acidic sites.[19−21] This bimodal behavior is unusual for mineral oxide interfaces and has been attributed to different hydrogen-bonding environments of the two silanol sites that lead to stark differences in acidity.[22,23]

Another feature of the silica–water interface that has long interested scientists is the sensitivity of dissolution and surface deprotonation processes to ionic strength[16,17,24,25] and electrolyte composition of the aqueous layer.[18,26−29] Regarding the latter, these specific ion effects reveal that not only the charge but also the polarizability of the ions in the aqueous phase can influence their properties.[30,31] For example, Dove and co-workers found that the dissolution rate of silica varied

Received: February 1, 2013
Revised: March 21, 2013
Published: March 22, 2013

  

depending on the identity of the solution-phase alkali and alkaline earth ions present.[24,27,28] They attributed this specific ion dissolution behavior to the ability of the ion to form inner-sphere interactions with the silica sites, which facilitated hydrolysis of the O−Si bond coordinated to the cation.[29] Regarding surface deprotonation, Ninham and co-workers[32] and Dove and Craven[33] examined the change in surface charge density using potentiometric methods over a narrow pH range for mesoporous silica and colloidal silica, respectively, dispersed in different alkali chloride solutions. Both reports found that the 6.5−8.5 pH range yielded different surface charge densities depending on the cation present, with potassium leading to the greatest density of charged sites on silica.

Our group has been interested in using second harmonic generation spectroscopy to monitor specific ion effects on acid−base equilibria at the planar silica/water interface. Recently, we monitored the deprotonation of the two types of acidic sites in the presence of different alkali chloride electrolytes over a wide pH range using SHG.[21] We found that the corresponding acid dissociation constants ($K_a$) for the two sites were very sensitive to the composition of the aqueous electrolyte, with $Na^+$ leading to the greatest effective $K_a$ and $Cs^+$ leading to the lowest effective $K_a$. We attributed this trend in effective $K_a$ values to the stronger interaction of the sodium with the siloxide sites in comparison to the larger, more polarizable cesium. Not only was the measured $K_a$ very sensitive to the nature of the electrolyte, but the population distribution of the two acidic sites also varied greatly depending on the alkali ion. Overall, these studies supported that specific interactions between the cation and siloxide sites, as well as interactions between the alkali chloride and water, influenced the resulting acid−base behavior of the surface.[21,33]

One outstanding question that remains is whether the identity of the halide influences the acid−base chemistry of the silica/water interface. Although halides are generally known to have more significant specific ion effects on the interfacial hydrogen-bonded structure of water at the air/water,[34,35] protein/water,[36] and polymer/water interfaces,[37] their influence has been much less explored on negatively charged surfaces like silica, where the point of zero charge occurs at pH 2.[38,39] To illustrate the former, both theoretical simulations and experimental studies have established that the air/water interface shows enhanced affinity for certain anions like iodide.[31,35,40] Cremer and co-workers found that neutral Langmuir−Blodgett (LB) films of polymers and peptides also have a higher affinity for iodide or bromide than chloride.[36,37,41] This affinity of more polarizable anions like iodide and bromide for neutral LB film interfaces has been attributed to the weak interactions of the larger halides with water that allow it to interact more strongly with the protein or polymer interface, primarily through dipole interactions.[37,41]

In contrast to these air/water and LB film/water investigations, there has been less focus on specific anion effects of halides on negatively charged mineral oxide surfaces. For the planar silica−water interface where the interfacial water structure is expected to play an important role, we would expect the influence of the halide identity to be significant. Herein we apply SHG spectroscopy to monitor the influence of the interfacial halide ions on the effective $pK_a$ of the acid−base equilibria as well as the bimodal distribution of the two surface acidic sites. Not only do we observe significant effects of the halide identity on the ratio of the more acidic to less acidic sites, but we also observe cooperative acid−base behavior that depends on the nature of the halide ion. To the best of our knowledge, such striking evidence of cooperative deprotonation processes has never before been observed at a mineral oxide interface. Understanding such behavior is key to predicting the surface charge density of silica over a wide pH range, which is essential to both accurate environmental modeling and materials applications using silica as the substrate.

## 2. EXPERIMENTAL SECTION

**2.1. Laser System and SHG Assembly.** A detailed description of the laser system used in these experiments can be found in our previously published work.[21] Briefly, the system consists of a femtosecond Ti:sapphire oscillator (Spectra-Physics, Mai Tai, 80 MHz) and a Nd:YLF laser (Spectra-Physics, Empower) used to seed and pump, respectively, a regeneratively amplified laser (Spitfire Pro, Spectra Physics, 1 kHz, 100 fs, 3.3 W). One-third of the Spitfire output is used to pump an optical parametric amplifier (Spectra-Physics OPA-800CF). The output from the OPA (tuned to 550 ± 2 nm) was then attenuated to 0.4 ± 0.1 μJ by a neutral-density filter (New Focus, cat. # 5215) and directed through a half-wave plate and polarizer for s-polarization selection, unless otherwise noted. The polarized light was focused onto the fused silica/water interface at an angle of 62° from surface normal near total internal reflection. The reflected second harmonic light generated at the interface was then passed through a color glass filter (Thorlabs) to remove the reflected fundamental light and focused onto a monochromator (Optometrics Corp., Mini-Chrom MC1-02) tuned to the second harmonic wavelength (275 nm). SHG was detected by a photomultiplier tube (PMT, Hamamatsu Photonics), and the electric response from the PMT was then amplified and counted with a gated photon counter (Stanford Research Systems). Before performing each experiment, the quadratic power dependence and SHG wavelength dependence were verified to ensure no optical damage was occurring at the interface.[9]

For all SHG measurements a freshly cleaned fused silica hemisphere (ISP optics, 1 in. diameter, QU-HS-25, UV-grade $SiO_2$) was placed on a custom-built Teflon cell so that the flat surface of the hemisphere was in contact with the aqueous phase. The silica/water interface was perpendicular to the surface of the laser table, and the aqueous phase was exposed so the pH could be routinely changed and monitored from the top.[21]

**2.2. Broadband Vibrational Sum Frequency Generation Experiments.** A detailed description of our broadband sum frequency generation setup is forthcoming.[42] Two-thirds of the output of the Spitfire Pro regeneratively amplified system described above (2.2 W) was also used to pump a TOPAS-C/NDFG optical parametric amplifier (Light Conversion). The resulting broadband infrared light was tuned from 3000 to 3600 $cm^{-1}$ to probe resonances of the O−H stretch of water at the interface. Visible light from the Spitfire (100 fs, $\lambda$ = 800 nm) was broadened to a picosecond pulse using a Fabry-Perot etalon (fwhm ∼10 $cm^{-1}$). The p-polarized femtosecond IR light (∼10−12 μJ/pulse) and the p-polarized picosecond visible light (∼10 μJ/pulse) were focused through a fused silica hemisphere (ISP optics, 1 in. diameter, IR-grade $SiO_2$), enclosed in the same type of sample cell holder as the SHG setup, onto the silica/water interface at angles of 66° and 64°, respectively, from surface normal. After spatially and temporally aligning the two fields, the sum frequency light emanating from the sample was recollimated, filtered with a bandpass filter to


dx.doi.org/10.1021/jp401164r | J. Phys. Chem. C 2013, 117, 8840−8850

remove residual 800 nm light (Chroma, HQ 617/70 M), passed through a polarizer to select p-polarized SFG, and focused onto a spectrograph (Acton SP-2556 imaging spectrograph, grating: 1800 grooves/mm with 500 nm blaze wavelength) connected to a thermoelectrically cooled, back-illuminated, charge-coupled device camera (Acton PIXIS 100B CCD digital camera system, 1340 × 100 pixels, 20 $\mu$m × 20 $\mu$m pixel size, Princeton Instruments). The ppp-polarization combination was selected as it is particularly sensitive to the amount of ordered interfacial water molecules.[43] Before performing an experiment, reference spectra were first collected using the same configuration with a gold-coated silica hemisphere with the IR centered at 3160, 3280, 3390, and 3500 $cm^{-1}$. Spectra at the same central wavelengths were measured for the silica/water interface. The spectra from the silica/water interface were normalized by summing the spectra and dividing this summed spectrum by the sum of the gold reference spectra following previous reports.[44]

**2.3. Surface Preparation.** The silica hemisphere was cleaned prior to use by sonicating it in Millipore water followed by methanol and then in water again. The flat surface of the hemisphere was covered with a few drops of freshly prepared commercial glass cleaner Nochromix (Godax Laboratories, 5% w/v solution in $H_2SO_4$) for 1 h followed by copious rinsing in Millipore water. Next, the hemisphere was rinsed thoroughly with Millipore water followed by sonication in water (5 min × 2), in methanol (5 min), and then in water again (5 min). After the hemisphere was allowed to dry in an oven at 100 °C for 10 min, it was cooled down to room temperature and then plasma cleaned (plasma cleaner, PDC-32G, Harrick Plasma) in air for 2−3 min.

**2.4. Materials.** Potassium bromide was purchased from Sigma-Aldrich. Sodium chloride (≥99%) and sodium hydroxide (≥97%) were purchased from EMD Chemicals Inc. Potassium chloride (≥99%) and potassium iodide (>99%) were purchased from Analchemia Canada Inc. Sodium iodide (>99.5%), potassium hydroxide (≥85%), sulfuric acid, and hydrochloric acid were obtained from Caledon Laboratories. Sodium bromide (>99.5%) was purchased from Fisher Chemical. All compounds were used without further purification. Ultrapure deionized (18.2 MΩ·cm) water was used shortly after deionization by a Milli-Q-Plus ultrapure water purification system (Millipore). The pH of all the solutions was measured with an Orion 2 star pH meter from Thermo Scientific using a double-junction Ag/AgCl electrode (Orion, 9107APMD). All experiments were performed with freshly prepared salt solutions.

**2.5. SHG pH Variation Experiments.** Prior to the start of an experiment, each sample was exposed to Milli-Q water until the SHG signal was optimized. As reported in our previously published paper,[21] separate experiments were performed for the lower and higher pH regions on different fresh samples to avoid any hysteresis.[45] Next, the water in the sample cell was completely replaced by ∼10 mL of the salt solution of interest that had been pH adjusted to 7 for the low-pH experiments or not pH adjusted for the high-pH experiments. This silica/electrolyte interface was allowed to equilibrate for 30 min while monitoring the SHG signal. After this equilibration time, aliquots of the corresponding acid or base solution with the same salt concentration (0.5 M) were added to adjust the pH by ∼0.3 pH units. At each new pH, the system was allowed to stand for ∼3 min to reach equilibrium, and then SHG was collected for ∼2 min. This step of changing the pH and measuring the corresponding SHG signal was repeated until the pH of the solution reached 12.5 for the high-pH titrations and reached 2 for the low-pH titrations. The normalized $E_{2\omega}$ was determined from $I_{2\omega}$ as described in our previous work.[21] The plot of normalized $E_{2\omega}$ versus solution pH was then fit with a sigmoid function. The inflection point determined by the fit is the $pH_{0.5}$ value equivalent to the $pK_a^{eff}$ according to the cooperative model. The listed $pK_a^{eff}$ values and the error represent the average of values determined from two or more experiments and the measured range of values, respectively. The cooperative number $n$ was determined by fitting $\log[\alpha(1-\alpha)]$ versus pH from $-1 < \log[\alpha(1-\alpha)] < 1$ with a line of best fit, where $\log[\alpha(1-\alpha)] = n\text{pH} - npK_a^{eff}$. All of the data for duplicate experiments were first compiled and then plotted to find $n$. The reported value is from the fit of the compiled data, and the error is the standard deviation reported from the fit.

**2.6. SFG pH Variation Experiments.** The SFG experiments were similarly conducted. First, SFG was measured for the silica/water interface without pH adjustment. The solution was then removed, and a 0.5 M NaI solution was added that had not been pH adjusted followed by monitoring of the SFG response. Next, a concentrated solution of NaOH (0.5 M NaI) was added dropwise to the aqueous phase until the desired basic pH was reached. SFG was once again measured. The low-pH experiments were performed in a similar manner on a different sample beginning with Millipore water. To illustrate the reproducibility in signal shape and intensity, we included both of the spectra at neutral pH (0.5 M NaI) that corresponded to the experiments at high and low pH. Each experiment was performed in duplicate to confirm the trends in SFG intensity change, and one representative set of data is shown in Figure 6.

## 3. RESULTS AND DISCUSSION

Owing to its intrinsic surface selectivity and sensitivity to interfacial charge, we selected SHG spectroscopy to monitor the influence of the interfacial halide ions on the acid−base behavior of the silica/water interface. SHG is a second-order nonlinear optical process that occurs in noncentrosymmetric environments. At the interface of fused (noncrystalline) silica and bulk water, second harmonic generation results when light of frequency $\omega$ interacts with the interface leading to an induced polarization, $P_{2\omega}$, that oscillates at twice the incident frequency. This oscillating polarization generates the second harmonic electric field, $E_{2\omega}$. At a neutral surface, $E_{2\omega}$ depends on the incident electric field, $E_{\omega}$, and the second-order susceptibility, $\chi^{(2)}$, which, within the electic dipole approximation, is only nonzero for noncentrosymmetric environments like interfaces. However, Eisenthal and co-workers demonstrated that $E_{2\omega}$ generated from a charged surface is also enhanced by a third static electric field, the magnitude of which depends on the third-order susceptibility, $\chi^{(3)}$.[19,20] Consequently, $E_{2\omega}$ can be expressed as

$$E_{2\omega} \propto P_{2\omega} = \chi^{(2)}E_{\omega}E_{\omega} + \chi^{(3)}E_{\omega}E_{\omega}\Phi_0 \quad (1)$$

where $\Phi_0$ is the interfacial potential arising from the surface charges. This $\chi^{(3)}$ technique has been widely used to monitor surface potentials,[46,47] electrostatic interactions,[48−51] and protonation/deprotonation processes[19,20,25,45,52−54] based on the second harmonic optical response that can be correlated with changes in the interfacial potential. To monitor acid−base processes in particular, $\chi^{(3)}$ experiments are often performed at


dx.doi.org/10.1021/jp401164r | J. Phys. Chem. C 2013, 117, 8840−8850

high electrolyte concentrations (~0.5 M) as the interfacial potential can be considered to vary linearly with the surface charge density at high ionic strength.[19−21,45,52] This linear dependence at high ionic strength arises from the collapse of the diffuse double layer, leaving only the compact Stern layer present that behaves like a parallel plate capacitor.[55] Under these conditions, $E_{2\omega}$ becomes a function of the potential within this condensed layer,[25] and the constant capacitance model can be used to relate the interfacial potential with the surface charge density.[56,57] Accordingly, decreases in SH signal, proportional to $|E_{2\omega}|^2$, can be correlated with a decrease in surface charge density (Scheme 1). As a result, a titration curve

**Scheme 1. Decreasing the pH and Protonating Surface Sites Decreases the SH Signal**[a]

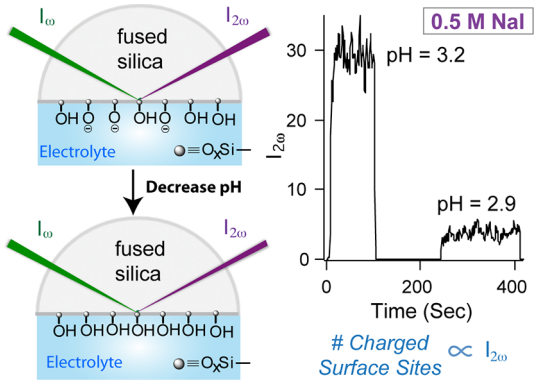


[a] $I_\omega$ is the incident intensity proportional to $|E_\omega|^2$. $I_{2\omega}$ is the SH signal intensity proportional to $|E_{2\omega}|^2$.

can be constructed simply by plotting the normalized $E_{2\omega}$ against solution pH, allowing the pH where half the sites have been deprotonated ($pH_{0.5}$) to be quantified.

Figure 1 illustrates representative acid−base titration profiles of the normalized SHG electric field versus solution pH. Consistent with previous reports, we observed two acid−base equilibria for the silica/water interface representative of two distinct acidic sites: one more acidic site that dissociated below pH 7 and the other less acidic site that dissociated above pH 7 (Figures 1A and 1B, respectively).[19−21,45] As the sodium halide was varied, the titration curves for both the more acidic (MA) and less acidic (LA) silanol groups exhibited very dramatic shifts in position. For example, NaCl electrolyte led to a $pH_{0.5}$ value for the MA sites of 4.06(4) and a $pH_{0.5}$ value for the LA sites of 8.6(1). In contrast, in the presence of NaI the corresponding values of $pH_{0.5}$ were 3.2(1) and 11.3(1) for the more acidic and less acidic sites, respectively. Unlike what was observed in the presence of different alkali chlorides where the trend in $pH_{0.5}$ was the same for both MA and LA sites,[21] the sodium halide data exhibited opposite trends for the two acidic groups. Specifically, NaI exhibited the lowest $pH_{0.5}$ value for the MA sites and the highest $pH_{0.5}$ for the LA sites. We concluded that, in the presence of NaI electrolyte, the extent of deprotonation at pH 7 represented a stable configuration for the interface such that further protonation or deprotonation was not favorable until extremely acidic or basic pH conditions were reached. Furthermore, the sharpnesses of the titration curves also varied significantly with the nature of the halide ion. This change in sharpness, which was not observed upon varying the cation identity, suggested that the halide ions not only influenced the stability of the acidic sites but also influenced the mechanism of the acid−base reaction.

As a point of comparison, we monitored the deprotonation of a solution-phase acid, bicarbonate, in the presence of 0.5 M sodium halide. In our previous work we found that the $pH_{0.5}$ values of this solution-phase acid varied slightly in the presence of different alkali chlorides, following the Hofmeister series $Li^+(pH_{0.5}) < Na^+(pH_{0.5}) < K^+(pH_{0.5}) < Cs^+(pH_{0.5})$.[21] For the anions, however, no difference in behavior was expected since there should be minimal interaction between the bicarbonate or carbonate anion and the halide. As anticipated, we did not observe a significant difference in $pH_{0.5}$ values for the different sodium halides (Figure 1C). This lack of influence of the halide anion on the solution-phase bicarbonate equilibrium contrasted sharply with the behavior of the silica/water interface, supporting that these specific halide effects are primarily interfacial effects, consistent with other specific ion studies.[41]

What makes the acid−base chemistry of the interface so sensitive to the identity of the halide? To address this question, we focused on the sharpness of the titration curves for iodide and bromide, indicative of cooperative acid−base processes. For acid−base reactions, positive cooperativity occurs when the deprotonation of one site makes the second deprotonation event thermodynamically more favorable, while a decrease in favorability is associated with negative cooperativity. The overall equilibrium constant that represents these cooperative sites with coupled equilibria can be expressed as

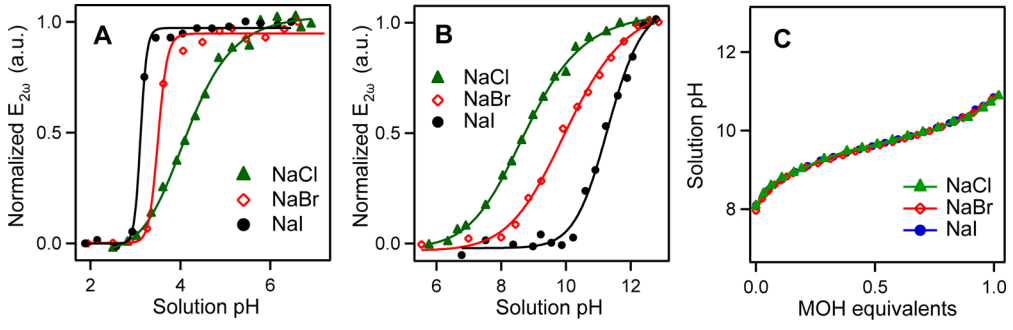


**Figure 1.** Representative titration curves for the silica/water interface in the presence of 0.5 M sodium halide salts. Normalized $E_{2\omega}$, which is proportional to the fraction of deprotonation of the silanol groups, is plotted as a function of (A) low pH and (B) high pH. The solid line is the sigmoidal fit of the titration data. (C) Titration curves for aqueous sodium bicarbonate in the presence of 0.5 M sodium halides, where pH is plotted against the equivalents of sodium hydroxide added.


dx.doi.org/10.1021/jp401164r | J. Phys. Chem. C 2013, 117, 8840−8850

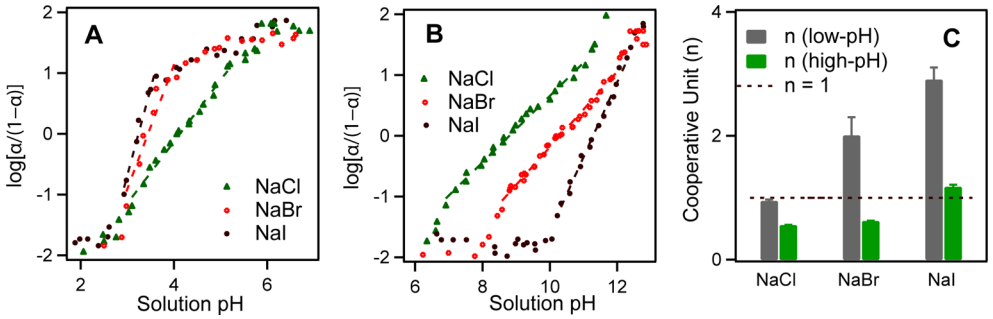


**Figure 2.** Representative plots of $\log[\alpha/(1-\alpha)]$ versus pH of the silica/water interface as a function of sodium halide (0.5 M) (A) at low pH and (B) at high pH. Dashed lines indicate the fit to the linear region of the modified Henderson–Hasselbalch equation, where the slope is equal to $n$. (C) Cooperative number $n$ corresponding to the transitions at low and high pH for the different sodium halides explored. The dashed line represents a noncooperative system ($n = 1$).

$$K_a^{\text{eff}} = K_1K_2K_3...K_n = \frac{[(\text{SiO}^-)_n][\text{H}_3\text{O}^+]^n}{[(\text{SiOH})_n]} \quad (2)$$

The term $n$ in this equation refers to the number of cooperative sites that interact and has been used to describe cooperativity in amphiphilic polypeptides.[58] After introducing this cooperative term, the modified Henderson–Hasselbach equation becomes

$$\text{pH} = \text{p}K_a^{\text{eff}} + \frac{1}{n}\log\left(\frac{\alpha}{1-\alpha}\right) \quad (3)$$

where $\alpha$ is the fraction of one type of surface site that is deprotonated, equivalent to normalized $E_{2\omega}$.[58] The $\text{pH}_{0.5}$ value at which point half of a given type of site is deprotonated corresponds to a $\log(\alpha/(1-\alpha))$ value of zero. Therefore, according to this model, the $\text{pH}_{0.5}$ that can be easily extracted from the titration profiles is equal to $\text{p}K_a^{\text{eff}}$.

There are numerous models for relating the composition of the electrolyte to the surface acidity of mineral oxides such as silica, some of which consider the effect of ion identity on surface deprotonation rather than cooperativity.[2,55,59−62] Owing to the clear influence of the anion on the sharpness of the titration profile, we utilized the approach presented above as it provides a simple physical model for understanding the influence of cooperativity on the acid–base chemistry of the surface. We note that in eq 3 we considered the solution pH rather than the surface pH to calculate the equilibrium constant $K_a^{\text{eff}}$. This constant based on the solution pH is sometimes referred to as the acid dissociation quotient $Q_a$ and is related to the $K_a$ derived from the surface pH by a potential-dependent term that accounts for enhancement or depletion of the surface concentration of $H_3O^+$ depending on the interfacial potential.[55] One advantage of using the solution pH is that it does not require knowledge of the absolute interfacial potential, which should differ at the same surface charge density depending on the ion identity and position within the electric triple layer.[62,63] Additionally, the solution pH transitions were so sharp in the presence of the larger halides that when the interfacial potential was plotted versus surface pH, the function deviated from sigmoidicity (see Supporting Information Figure S1). Finally, as discussed in our previous work, the apparent (noncooperative) $K_a$ of the surface also reflects interactions between the cations and the siloxide sites.[21] In these specific cation studies the overall equilibrium expression for the apparent $K_a$ included the cation concentration (where $K_a = [\text{SiO}^-\text{M}^+][\text{H}_3\text{O}^+]/[\text{SiOH}][\text{M}^+]$). As the cation surface concentration also depends on the interfacial potential, to a first approximation the potential dependence of the surface hydronium concentration and surface cation concentration cancel out in the final equilibrium expression. The contribution of the salt concentration to the measured $K_a$ is systematic as the salt concentration is kept constant for all of the different electrolytes explored. Here we do not implicitly describe the salt dependence within the equilibrium expression but rather the effect of cooperativity. As a result, we focus our discussion on the trends in $K_a$ rather than their absolute values.

To quantify cooperativity using eq 3, we determined the value of $\log(\alpha/(1-\alpha))$ from compiled experiments consisting of normalized $E_{2\omega}$ vs pH (Figure 2). The slope equal to $n$ was measured for the linear region of the trace (where $1 \geq \log[\alpha/(1-\alpha)] \geq -1$).[58] The values of $n$ for the MA and LA sites are listed in Table 1 and increase in the order $n$(NaCl) < $n$(NaBr) < $n$(NaI). For the more acidic silanol groups deprotonated below pH 7, we observed no cooperativity in the presence of NaCl ($n \approx 1$), while the presence of NaBr and NaI led to cooperative numbers of ~2 and 3, respectively (Table 1). For the experiments performed at higher pH, NaI led to a cooperative number close to 1 (1.17(4)), yet NaBr and NaCl yielded $n$ values of 0.62(1) and 0.55(1), respectively. Generally, these values indicated that the more acidic sites exhibited positive cooperativity ($n > 1$) and the less acidic sites exhibited negative cooperativity ($n < 1$).

**Table 1. Parameters for the More Acidic (MA) and Less Acidic (LA) Sites Based on the Cooperative Equilibrium Model**

| | more acidic (MA) sites | | | less acidic (LA) sites | | |
|---|---|---|---|---|---|---|
| salt | $\text{p}K_a^{\text{eff}}$ | $n$ | $\text{p}K_a$ | $\text{p}K_a^{\text{eff}}$ | $n$ | $\text{p}K_a$ |
| NaCl | 4.06(4) | 0.94(3) | 4.0 | 8.6(1) | 0.55(1) | 10.0 |
| NaBr | 3.4(2) | 2.0(3) | 4.3 | 10.3(2) | 0.62(1) | 11.4 |
| NaI | 3.2(1) | 2.9(2) | 4.3 | 11.3(1) | 1.17(4) | 11.0 |
| KCl | 4.9(3) | 0.99(3) | 4.9 | 10.2(2) | 0.50(1) | 11.9 |
| KBr | 4.1(2) | 2.1(1) | 5.0 | 11.1(2) | 0.75(4) | 11.7 |
| KI | 3.4(2) | 2.9(3) | 4.5 | 11.5(2) | 1.10(6) | 11.3 |

The relationship between $\text{p}K_a^{\text{eff}}$ and $\text{p}K_a$ can be determined from $n$ with the following phenomenological equation:[58]

$$\Delta\text{p}K = \frac{\Delta G_{\text{interaction}}}{2.3RT}\left(1 - \frac{1}{n}\right) = \pm 1.74\left(1 - \frac{1}{n}\right) \quad (4)$$

Here $\Delta G_{\text{interaction}}$ stems from interactions between neighboring sites and is usually on the order of 4RT.[58] Consequently, we


dx.doi.org/10.1021/jp401164r | J. Phys. Chem. C 2013, 117, 8840−8850

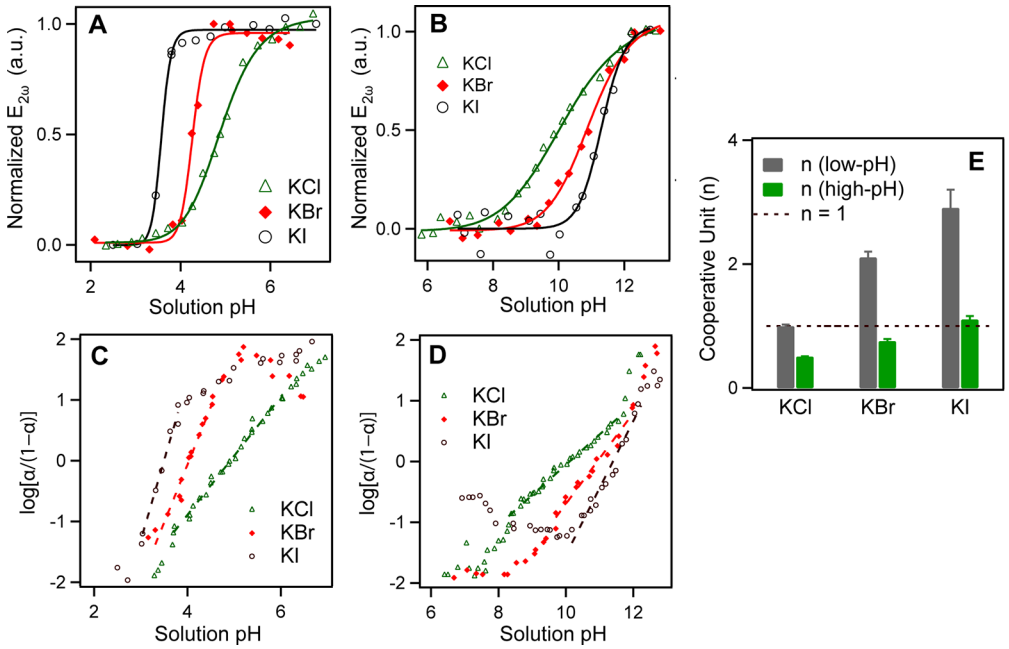


**Figure 3.** Representative titration curves for the (A) more acidic and (B) less acidic sites of the silica/water interface in the presence of different potassium halides. Log$[\alpha(1-\alpha)]$ as a function of (C) low solution pH and (D) high solution pH for the silica/water interface with different potassium halide electrolytes. The dashed lines represent the fit to the linear portion of the trace ($-1 < \log[\alpha(1-\alpha)] < 1$). (E) The $n$ values for the more acidic and less acidic sites determined from the plots in (C) and (D). The dashed line marks $n = 1$, which is the $n$ value corresponding to a noncooperative system.

can determine the intrinsic p$K_a$ of the different sites according to

$$pK_a = pK_a^{eff} - \Delta pK \quad (5)$$

From eqs 4 and 5, we see that p$K_a$ is equal to p$K_a^{eff}$ for a noncooperative system.

Using eqs 4 and 5, this intrinsic p$K_a$ was calculated for the two types of acidic silanol groups (Table 1). For the more acidic silanol groups, increasing cooperativity led to a decrease in p$K_a^{eff}$ and consequently a negative $\Delta pK$, indicating that $\Delta G_{interaction}$ was also negative and attractive. These attractive interactions could stem from hydrogen bond formation among neighbors or more favorable surface interactions with the compact Stern layer upon surface deprotonation. In contrast, increasing cooperativity led to an increase in p$K_a^{eff}$ for the less acidic sites, indicating that $\Delta pK$ was positive and that $\Delta G_{interaction}$ was positive and repulsive, which we attribute to charge−charge repulsion among neighboring sites (vide infra). For the more acidic silanol groups, the p$K_a$ values were very similar yielding an average value of 4.2, ranging in value from 4.0 to 4.3, which indicated that the differences in p$K_a^{eff}$ for the different sodium halide solutions were due primarily to differences in cooperativity and not differences in the intrinsic acidity of these MA sites. In contrast, the p$K_a$ values were not consistent for the different sodium halide salts for the less acidic surface sites as indicated by the large range of p$K_a$ values (10.0−11.4). This disagreement with the cooperative model indicated that the acidity of these LA surface sites was influenced by other factors in addition to cooperativity.

To test whether the presence of sodium was critical to the observed halide behavior, we performed similar experiments using potassium halides (Figure 3). The potassium halides yielded very similar trends in both the cooperative unit and the trend in p$K_a$ values. Indeed, the cooperative numbers were within error for both the sodium and potassium salts of the like halide (Table 1). This similarity suggested that it was the identity of the halide and not the alkali ion that influenced the cooperative behavior. Alternatively, it is possible that both the sodium and potassium possess different water matching affinities[64] than the polarizable bromide and iodide anions, and this mismatch may facilitate formation of a cooperative interfacial structure. If this were the case, larger more polarizable cations similarly matched with the larger anions might lead to less cooperative behavior, which will be examined in future work. The intrinsic p$K_a$ values, however, varied for the sodium and potassium salts. Our previous work comparing the behavior of alkali chlorides on the acid−base behavior of silica indicated that the affinity of the cation for the siloxide determined its apparent p$K_a$.[21] Here we also considered the theory of matching water affinities[64] and concluded that sodium interacted most strongly with the siloxide sites owing to their similar affinity for water. The same trend is observed herein, where all of the sodium salts led to lower p$K_a$ values than the corresponding potassium salts, which we attribute again to stronger sodium−siloxide interactions.

Both the potassium and sodium iodide systems exhibited positive cooperativity for the more acidic sites ($n$ = 0.94−2.9) and negative cooperativity for the less acidic sites ($n$ = 0.55−1.17) (Table 1). As shown in Figure 4, the cooperative number for the MA sites is strongly correlated with both the size of the anion (based on the ionic area) and the free energy of hydration. The larger the anion and the smaller the energy of hydration, the more positively cooperative the system. This trend in $n$ values suggests that the larger anions interacted with multiple silanol groups, which led to coupled acid−base behavior among neighbors (Scheme 2). This could in part be due to its larger ionic area that facilitated cooperative interactions (Figure 4A). Additionally, the ability of iodide in particular to become partially desolvated owing to its weak


dx.doi.org/10.1021/jp401164r | J. Phys. Chem. C 2013, 117, 8840−8850

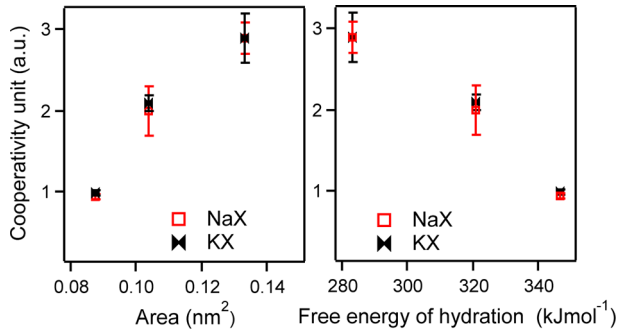


**Figure 4.** Cooperativity as a function of ionic area and free energy of hydration of the respective anions.

**Scheme 2. Positively Cooperative Dissociation of More Acidic Sites**

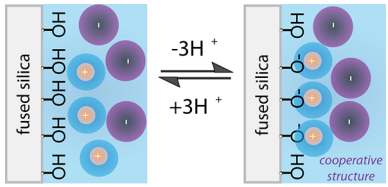


interactions with water makes it more favorable for it to partition to the interface, which has been used to explain its greater affinity for hydrophobic or neutral surfaces (Figure 4B).[37,41] At the negatively charged mineral oxide interface, we propose that a cooperative compact layer forms consisting of stabilizing clusters of siloxide−alkali complexes that are then capped with an iodide layer that favors surface interactions more so than those with bulk water (Scheme 2). The position of the water molecules in this compact layer is not known, although our previous work indicated that sodium and potassium may form a partially dehydrated ion interaction with siloxide sites.[21]

Thus far we have considered the behavior of the two different sites independently. As previously discussed, the different acidities of the sites have been correlated with different hydrogen-bonding environments of the silanol groups. For example, one recent MD-DFT study indicated that the more acidic sites donated hydrogen bonds to water, whereas the less acidic sites donated hydrogen bonds to neighboring silanols.[23] We reasoned that the presence of different ions could change the hydrogen bonding of the silanols and that of interfacial water, which in turn could influence the bimodal distribution of more and less acidic sites. The relative distribution of the two sites can be calculated from the normalized interfacial potential using the relative change in $E_{2\omega}$ at low and high pH as described elsewhere.[21] Thus, experiments at low and high pH were performed separately to avoid hysteresis in these systems[45] and were combined by relating $E_{2\omega}$ to the average value at neutral pH ($rE_{2\omega}$) according to

$$rE_{2\omega} = \frac{E_{2\omega}}{E_{2\omega}(\text{pH } 7)} \tag{6}$$

The normalized interfacial potential (N-$\Phi_0$) was then determined by compiling multiple high- and low-pH experiments:

$$\text{N-}\Phi_0 = \frac{rE_{2\omega} - rE_{2\omega}(\text{pH } 2)}{rE_{2\omega}(\text{pH } 12) - rE_{2\omega}(\text{pH } 2)} \tag{7}$$

The compiled data consisting of all possible combinations of low- and high-pH data sets were smoothed and then used to determine N-$\Phi_0$ as a function of pH as depicted in Figure 5A,B

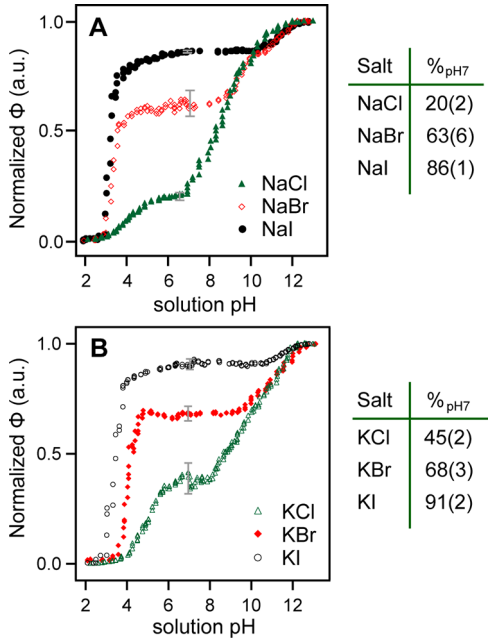


| Salt | $\%_{pH7}$ |
|---|---|
| NaCl | 20(2) |
| NaBr | 63(6) |
| NaI | 86(1) |

| Salt | $\%_{pH7}$ |
|---|---|
| KCl | 45(2) |
| KBr | 68(3) |
| KI | 91(2) |

**Figure 5.** Normalized Φ, which is proportional to the relative surface charge density, as a function of pH in the presence of (A) sodium halides and (B) potassium halides. The tables represent the relative distribution of the two acidic sites at these silica/halide interfaces as the percent deprotonated at pH 7 ($\%_{pH\ 7}$) is equivalent to the percentage of more acidic sites.

(5 point box smoothing function). To ensure that our method for combining the low- and high-pH data was reasonable, we compared the N-$\Phi_0$ values with the $E_{2\omega}$ of the electrolyte interface at neutral pH referenced to that of Millipore water, which represented a common starting point for every experiment. There is a general correlation between the $E_{2\omega}$ referenced to water and the trend in N-$\Phi_0$ values, indicating that the presence of the ions does lead to a different extent of deprotonation at neutral pH and accordingly a change in bimodal distribution (see Supporting Information, Figure S2).

Figure 5 illustrates the change in interfacial potential over the entire pH range studied. If we once again consider the constant capacitance model, then the normalized interfacial potential (N-$\Phi_0$) should directly reflect the fraction deprotonated of the surface as a function of pH. Consequently, the percent deprotonated at neutral pH ($\%_{pH\ 7}$), or N-$\Phi_0$(pH 7) × 100%, is equivalent to the percentage of more acidic sites (MA %), as this pH lies between the two deprotonation equilibria. For the silica/water interface in the presence of the NaCl electrolyte, the corresponding MA% was 20(2)% (Figure 5A), consistent with what was reported by Eisenthal and co-workers.[19] In contrast, in the presence of NaBr electrolyte, the MA% increased to 63(6)%. The trend continued, with the NaI system exhibiting the greatest percentage of more acidic sites of 86(1)%. A very similar trend was observed for the potassium halides as well (Figure 5B). Consequently, we infer that the silica surface at neutral pH can possess drastically different surface charge densities depending on the halide present. Significant differences in MA% were also observed for the various alkali chlorides (from 20 to 60%),[21] but the trends for


dx.doi.org/10.1021/jp401164r | J. Phys. Chem. C 2013, 117, 8840−8850

the halide series are even more substantial. Additionally, for the alkali chloride series the MA% values increased with a decrease in the free energy of cation hydration with the exception of lithium.[21] Similarly, we observe that MA% increased as the free energy of hydration decreased for the halides. This observation supports that the ions that do not favor strong interactions with water are able to influence the hydrogen-bonding structure at the interface in a way that prefers the formation of MA over LA sites.

The differences in N-$\Phi_0$ values for the different electrolytes also shed light on why the cooperative model failed to account for the intrinsic differences in surface acidity of the LA sites shown by the p$K_a$ values (Table 1). Now we see that the p$K_a^{eff}$ values for the less acidic sites are directly correlated with how charged the surface is at pH 7, when essentially all of the LA sites are still protonated. For example, in the presence of NaCl electrolyte only 20% of the surface sites were deprotonated at pH 7. Consequently, the p$K_a^{eff}$ of the remaining 80% of sites was the lowest (8.6(1)), meaning they were the most acidic or easily deprotonated. For the NaBr, the amount of surface charges was 63(6)% at pH 7, leading to a p$K_a^{eff}$ for the remaining LA sites of 10.3(2). The NaI exhibited both the greatest amount of surface charges at neutral pH (86(1)%) and the highest LA p$K_a^{eff}$ value (11.3(1)). These results reveal that the greater the initial charge of the interface, the more difficult the deprotonation of the remaining LA sites, owing to charge repulsion with the high density of siloxides already present.

The different extent of surface charging at neutral pH also accounts for the trend in $n$ values for the LA sites. For the interface in the presence of NaCl, the remaining LA sites represented 80% of the surface sites. Consequently, there were many LA sites that neighbored one another. The close arrangement of the protonated sites led to negative cooperativity ($n$ = 0.52), where the deprotonation of one site increased the energetic penalty for deprotonation of the neighbor. Similarly, the NaBr electrolyte/silica interface exhibited negative cooperativity for the LA sites that made up 37% of the surface, but to a lesser extent than the NaCl system, given the lower density of LA sites. For the NaI electrolyte interface, however, the density of LA sites was so low (14%) that deprotonation of these LA sites occurred in a non-cooperative manner with no nearest-neighbor interactions ($n \sim 1$). We reason that the LA sites exhibited charge repulsion unlike the MA sites because of the structure of the compact Stern layer that cannot further compensate for the increase in lateral repulsion with increasing surface deprotonation.

To gain some insights into the structure of this compact Stern layer, we turned to vibrational sum frequency generation (SFG), a complementary nonlinear optical technique that can be used to probe the amount of ordered water at the interface. In these experiments, two electric fields were incident on the interface: one in the visible and the other in the infrared (Figure 6A). When the IR frequency is in resonance with vibrational modes associated with ordered molecules at the interface, the second-order susceptibility $\chi^{(2)}$ becomes large, leading to an increase in the electric field at the sum of the two incident frequencies ($E_{SF}$). As in SHG, within the electric dipole approximation the second-order susceptibility $\chi^{(2)}$ is only nonzero for noncentrosymmetric environments. Consequently, only ordered water molecules contribute to the resonantly enhanced part of the $\chi^{(2)}$ term:

$$E_{SF} \propto P_{SF} = \chi^{(2)} E_{Vis} E_{IR} + \chi^{(3)} E_{Vis} E_{IR} \Phi_0 \quad (8)$$

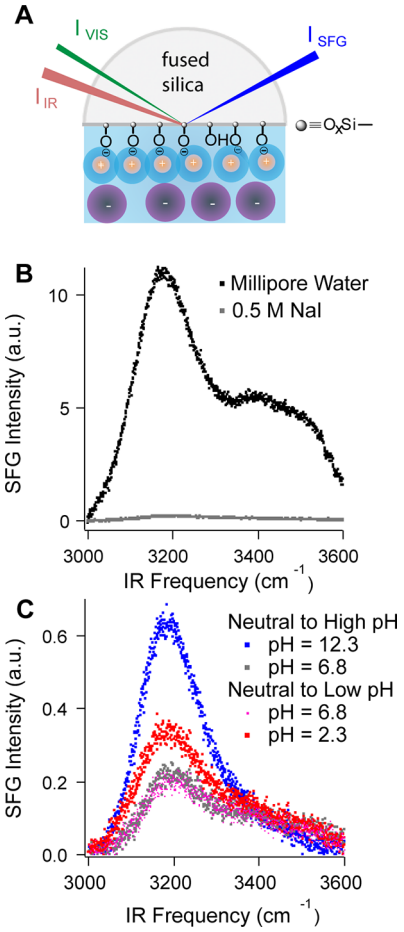


**Figure 6.** (A) Schematic illustrating sum frequency generation at the silica/aqueous interface. $I_{VIS}$ and $I_{IR}$ are the incident visible and infrared light intensities from the tunable laser assembly. $I_{SFG}$ is the intensity of the sum frequency signal. (B) Vibrational SFG spectra of the silica/Millipore water interface (black trace) and the silica/0.5 M NaI electrolyte interface (gray trace) at neutral pH. (C) Vibrational SFG spectra of the silica/0.5 M NaI electrolyte interface at different pH. The spectrum at neutral pH was measured on a fresh sample (gray and pink traces) before adjusting the electrolyte to high or low pH (blue and red, respectively). The ppp-polarization combination was used to monitor the amount of ordered water.[43]

In these SFG experiments, we utilized a femtosecond IR pulse that is broad in the frequency domain and a picosecond visible pulse that is narrow in the frequency domain. This common strategy for broadband SFG allows multiple resonant frequencies to be probed simultaneously, decreasing the amount of time required to capture a SFG spectrum.[67]

Figure 6B illustrates the SFG spectra of the silica/water interface at neutral pH in the presence and absence of 0.5 M NaI. The addition of sodium iodide led to a substantial decrease in SFG signal (~30−40-fold), much more so than that observed by Hore and co-workers for sodium chloride (~3-fold)[17] although in those studies a different polarization combination was used than for our experiments (ssp), so the changes in signal cannot be directly compared. The observed 30−40-fold decrease in SFG signal upon adding sodium iodide was also in stark contrast to the SHG experiments, where we saw on average a 2.5-fold *increase* in SHG intensity upon changing the aqueous solution from Millipore water to 0.5 M NaI at neutral pH. This difference in signal suggests that


dx.doi.org/10.1021/jp401164r | J. Phys. Chem. C 2013, 117, 8840−8850

nonresonant SHG and resonantly enhanced SFG are sensitive to different properties of the interface, which will be discussed in greater detail below. Finally, the significant decrease in the amount of ordered water in the presence of iodide at the negatively charged interface is very different than the trends observed for iodide interacting with the air/water[66] and neutral air/polymer[37] and protein interfaces.[36] For these neutral interfaces, it is reasoned that iodide partitioning leads to an increase in interfacial potential and consequently the amount of ordered water.[37] In our experiments, sodium iodide decreased the signal through a combination of screening and the displacement or disordering of interfacial water, which is consistent with the formation of a compact cooperative Stern layer that has less ordered water molecules.

At high electrolyte concentrations (>0.1 M), Hore and co-workers have shown that the resonant $\chi^{(2)}$ term associated with the aligned, oriented water in the compact Stern layer contributes more to the signal than the $\chi^{(3)}\Phi_0$ term, which is diminished by the short Debye length at these high salt concentrations.[17] To determine whether the amount of aligned, oriented water molecules in the compact Stern layer was affected by pH at these high NaI concentrations, we varied the pH from neutral to high pH and from neutral to low pH while maintaining the same electrolyte concentration as was done in the SHG titration experiments. The results are shown in Figure 6C. Unlike the trend observed by SHG, where the SHG signal exhibited a large decrease from neutral to low pH and a small increase from neutral to high pH, for the SFG spectra the signal intensity increased at both high *and low* pH compared with that at neutral pH. These results indicated that the amount (or net orientation) of ordered interfacial water within the compact Stern layer did vary with pH. As discussed previously, the presence of NaI led to the formation of a cooperative structure between the surface, cations, and anions that stabilized the dissociated MA sites and the protonated LA sites (Scheme 2). We reason that this cooperative structure present at neutral pH displaced more interfacial water molecules than the Stern layer present at low or high pH. Consequently, the SFG intensity, which is proportional to the amount of aligned water, was lowest at neutral pH.

We also note that the peak in the SFG spectra at ~3200 $cm^{-1}$ associated with high-coordinate water dominated at all pH conditions and was particularly enhanced at high pH. A very similar trend in the shape of the SFG spectra was observed for the silica/electrolyte interface under different pH conditions in the presence of 0.1−0.5 M NaCl.[13] The small contribution of signal at 3400 $cm^{-1}$, which is associated with low-coordinate water, suggested that high salt concentrations particularly perturb the weakly coordinated water. Interestingly lower alkali chloride salt concentrations have been found to diminish the peak at 3200 $cm^{-1}$ more so than that at 3400 $cm^{-1}$.[18] Future work will examine the affect of lower iodide salt concentrations on the SFG spectra at the silica/electrolyte interface.

Finally, the very different trends in signal intensity for resonantly enhanced SFG, where $\chi^{(2)}$ dominates, and non-resonant SHG, where $\chi^{(3)}\Phi_0$ should dominate, support that the changes in signal observed by SHG indeed stem from the $\chi^{(3)}\Phi_0$ term. This is important for our analysis as it allows us to relate all changes in signal to $\Phi_0$. Moreover, it lends further support to the first reports on the $\chi^{(3)}$ technique,[9,19,20] which indicated that the nonresonant $\chi^{(2)}$ represented in eq 2, which also stems from the ordered, oriented water molecules, is much smaller than $\chi^{(3)}\Phi_0$ and therefore can be considered to remain invariant with changing pH. One question that might arise is whether iodide and bromide directly contribute to the interfacial potential instead of increasing the magnitude of the potential by facilitating deprotonation of the surface. Alternatively, $I^-$ or $Br^-$ could contribute to $\chi^{(2)}$ due to their greater polarizability. Previous work has indicated that polarizable anions like iodide interact more strongly with neutral rather than charged interfaces,[36] which should lead to the greatest amount of iodide binding near the point of zero charge (pH 2). Yet, upon adding sodium iodide to the interface at low pH near the point of zero charge, we did not observe signal enhancement (data not shown). In contrast adding sodium iodide to the silica/water interface at neutral pH led to a ~2.5-fold signal increase (or an increase in $E_{2\omega}$ of ~1.6 (Figure S2)), which is consistent with our interpretation that iodide changes the interfacial potential indirectly by promoting surface deprotonation rather than directly contributing to the potential or $\chi^{(2)}$.

We note, however, that other factors could still affect the observed change in signal or intrepretation of the SHG experiments. For example, if changes in nonresonant $\chi^{(2)}$ arising from changes in the composition of the Stern layer were not completely overwhelmed by changes in $\chi^{(3)}\Phi_0$, the resulting signal might depend on the polarization of the incident light. We did observe differences for the silica/$NaI_{(aq)}$ interface in the N-$\Phi_0$ vs pH data upon changing the incident light to p-polarization, which suggested that changes in $\chi^{(2)}$ did contribute slightly to the changes in signal (Figure S3). Yet, these differences were small when compared with the differences observed among the halides, such that it is reasonable to relate the change in signal to changes in the interfacial potential. Second, we assumed the constant capacitance model, which states that the interfacial potential and surface charge density are proportional, was valid even as the surface charge density approached zero. Changes in the compact Stern layer structure, particularly from zero to low charge densities, could cause the capacitance to change as a function of pH, which would affect our determination of the percent deprotonated and the $pK_a$ values. However, at the high salt concentrations used, model calculations support that the potential and surface charge density vary linearly even to the point of zero charge,[55] and therefore the constant capacitance model represents an appropriate starting point for analyzing these effects. Lastly, although the salt samples used were of high purity, there is always concern particularly with iodide that surface-active impurities contribute to the observed signal, which cannot be completely ruled out. Nevertheless, the fact that the $pK_a^{eff}$ and the cooperative unit for both the less acidic and more acidic sites follow strong trends with respect to the halide supports that the signal originates primarily from the acid−base chemistry of the silica/water interface. Moreover, the strong correlation between the amount of charge at pH 7 and the $pK_a$ and cooperativity of the remaining less acidic sites provides further indication that the changes in SH E-field observed herein primarily stem from deprotonation processes at the interface.

## 4. CONCLUSION

We have observed that sodium and potassium halides exhibit pronounced specific ion effects on the acid−base chemistry of the mineral oxide interface. The large influence of the halide is remarkable given the net negative charge on silica at all pH values explored in this study (point of zero charge = 2−3). This


dx.doi.org/10.1021/jp401164r | J. Phys. Chem. C 2013, 117, 8840−8850

work suggests that the larger halides formed structures at the interface that facilitated positive cooperativity between neighboring silanol groups for the more acidic sites. The larger, more polarizable halides also led to a significant shift in the bimodal distribution of silanol sites, such that the more acidic sites dominated. Consequently, the interfacial potential (and the corresponding surface charge density) at neutral pH increased significantly as the halide was varied from chloride to bromide to iodide. Finally, these experiments indicate that the influence of the halide must also be considered over a wide pH range to accurately model the surface charge density of negatively charged surfaces, which has major ramifications for modeling pollutant transport, weathering, and other environmental processes.[2,3] We are currently monitoring the specific ion effects at lower salt concentrations, the results of which are forthcoming.

## ■ ASSOCIATED CONTENT

### Ⓢ Supporting Information

Experiments illustrating the interfacial potential versus the surface pH, the $E_{2\omega}$ of the electrolyte referenced to that of pure water, the effect of incident polarization, and data from the individual experiments. This material is available free of charge via the Internet at http://pubs.acs.org.

## ■ AUTHOR INFORMATION

### Corresponding Author

*E-mail: gibbsdavis@ualberta.ca.

### Notes

The authors declare no competing financial interest.

## ■ ACKNOWLEDGMENTS

We thank Dr. Hong-Fei Wang (PNNL), Dr. Paul Cremer (Penn State), Dr. R. Kramer Campen (Fritz Haber Institute), and Dr. Franz Geiger (Northwestern) for helpful discussions. We also acknowledge the Natural Sciences and Engineering Research Council of Canada and the Canada Foundation for Innovation for funding.

## ■ REFERENCES

(1) Sposito, G. *The Surface Chemistry of Soils*; Oxford University Press: New York, 1984.
(2) Stumm, W.; Morgan, J. J. *Aquatic Chemistry: Chemical Equilibria and Rates in Natural Waters*, 3rd ed.; Wiley: New York, 1995.
(3) Langmuir, D. *Aqueous Environmental Geochemistry*; Prentice-Hall: Upper Saddle River, NJ, 1997.
(4) Iler, R. K. *Chemistry of Silica - Solubility, Polymerization, Colloid and Surface Properties and Biochemistry*; John Wiley & Sons: New York, 1979.
(5) Dove, P. M.; Rimstidt, J. D. In *Reviews in Mineralogy Series: The Silica Polymorphs*; Heaney, P., Prewitt, C., Gibbs, G., Eds.; Mineralogical Society of America: Washington, DC, 1994; Vol. *29*, p 259.
(6) Sahai, N. *Environ. Sci. Technol.* **2002**, *36*, 445.
(7) Liu, D.; Ma, G.; Allen, H. C. *Environ. Sci. Technol.* **2005**, *39*, 2025.
(8) Corn, R. M.; Higgins, D. A. *Chem. Rev.* **1994**, *94*, 107.
(9) Eisenthal, K. B. *Chem. Rev.* **1996**, *96*, 1343.
(10) Gopalakrishnan, S.; Liu, D.; Allen, H. C.; Kuo, M.; Shultz, M. J. *Chem. Rev.* **2006**, *106*, 1155.
(11) Schrödle, S.; Richmond, G. L. *J. Phys. D: Appl. Phys.* **2008**, 41.
(12) Verreault, D.; Hua, W.; Allen, H. C. *J. Phys. Chem. Lett.* **2012**, *3*, 3012.
(13) Du, Q.; Freysz, E.; Shen, Y. *Phys. Rev. Lett.* **1994**, *72*, 238.
(14) Li, I.; Bandara, J.; Shultz, M. J. *Langmuir* **2004**, *20*, 10474.
(15) Ostroverkhov, V.; Waychunas, G.; Shen, Y. *Phys. Rev. Lett.* **2005**, 94.
(16) Jena, K. C.; Hore, D. K. *J. Phys. Chem. C* **2009**, *113*, 15364.
(17) Jena, K. C.; Covert, P. A.; Hore, D. K. *J. Phys. Chem. Lett.* **2011**, *2*, 1056.
(18) Yang, Z.; Li, Q.; Chou, K. C. *J. Phys. Chem. C* **2009**, *113*, 8201.
(19) Ong, S.; Zhao, X.; Eisenthal, K. B. *Chem. Phys. Lett.* **1992**, *191*, 327.
(20) Zhao, X.; Ong, S.; Wang, H.; Eisenthal, K. B. *Chem. Phys. Lett.* **1993**, *214*, 203.
(21) Azam, M. S.; Weeraman, C. N.; Gibbs-Davis, J. M. *J. Phys. Chem. Lett.* **2012**, 1269.
(22) Leung, K.; Nielsen, I. M. B.; Criscenti, L. J. *J. Am. Chem. Soc.* **2009**, *131*, 18358.
(23) Sulpizi, M.; Gaigeot, M.-P.; Sprik, M. *J. Chem. Theory Comput.* **2012**, *8*, 1037−1047.
(24) Icenhower, J. P.; Dove, P. M. *Geochim. Cosmochim. Acta* **2000**, *64*, 4193.
(25) Campen, R. K.; Pymer, A. K.; Nihonyanagi, S.; Borguet, E. *J. Phys. Chem. C* **2010**, *114*, 8465.
(26) Sonnefeld, J. *Colloid Polym. Sci.* **1995**, *273*, 932.
(27) Dove, P. M. *Geochim. Cosmochim. Acta* **1999**, *63*, 3715.
(28) Karlsson, M.; Craven, C.; Dove, P. M.; Casey, W. H. *Aqua. Geochem.* **2001**, *7*, 13.
(29) Wallace, A. F.; Gibbs, G. V.; Dove, P. M. *J. Phys. Chem. A* **2010**, *114*, 2534.
(30) Lyklema, J. *Chem. Phys. Lett.* **2009**, *467*, 217.
(31) Parsons, D. F.; Bostrom, M.; Nostro, P. L.; Ninham, B. W. *Phys. Chem. Chem. Phys.* **2011**, *13*, 12352.
(32) Salis, A.; Parsons, D. F.; Bostrom, M.; Medda, L.; Barse, B.; Ninham, B. W.; Monduzzi, M. *Langmuir* **2010**, *26*, 2484.
(33) Dove, P. M.; Craven, C. M. *Geochim. Cosmochim. Acta* **2005**, *69*, 4963.
(34) Jungwirth, P.; Tobias, D. J. *Chem. Rev.* **2006**, *106*, 1259.
(35) Jungwirth, P.; Winter, B. *Annu. Rev. Phys. Chem.* **2008**, *59*, 343.
(36) Chen, X.; Flores, S. C.; Lim, S.-M.; Zhang, Y.; Yang, T.; Kherb, J.; Cremer, P. S. *Langmuir* **2010**, *26*, 16447.
(37) Chen, X.; Yang, T.; Kataoka, S.; Cremer, P. S. *J. Am. Chem. Soc.* **2007**, *129*, 12272.
(38) Franks, G. V. *J. Colloid Interface Sci.* **2002**, *249*, 44.
(39) Flores, S. C.; Kherb, J.; Cremer, P. S. *J. Phys. Chem. C* **2012**, *116*, 14408−14413.
(40) Petersen, P. B.; Saykally, R. J. *Annu. Rev. Phys. Chem.* **2006**, *57*, 333.
(41) Zhang, Y.; Cremer, P. *Curr. Opin. Chem. Biol.* **2006**, *10*, 658.
(42) Weeraman, C. N.; Azam, M. S.; Gibbs-Davis, J. M. 2013, manuscript in preparation.
(43) Yeganeh, M. S.; Dougal, S. M.; Pink, H. S. *Phys. Rev. Lett.* **1999**, *83*, 1180.
(44) Ding, F.; Hu, Z.; Zhong, Q.; Manfred, K.; Gattass, R. R.; Brindza, M. R.; Fourkas, J. T.; Walker, R. A.; Weeks, J. D. *J. Phys. Chem. C* **2010**, *114*, 17651.
(45) Gibbs-Davis, J. M.; Kruk, J. J.; Konek, C. T.; Scheidt, K. A.; Geiger, F. M. *J. Am. Chem. Soc.* **2008**, *130*, 15444.
(46) Yan, E. C. Y.; Liu, Y.; Eisenthal, K. B. *J. Phys. Chem. B* **1998**, *102*, 6331.
(47) de Beer, A.; Campen, R.; Roke, S. *Phys. Rev. B* **2010**, *82*, 235431.
(48) Hayes, P. L.; Malin, J. N.; Jordan, D. S.; Geiger, F. M. *Chem. Phys. Lett.* **2010**, *499*, 183.
(49) Holland, J. G.; Malin, J. N.; Jordan, D. S.; Geiger, F. M. *J. Am. Chem. Soc.* **2011**, *133*, 2567.
(50) Jordan, D. S.; Malin, J. N.; Geiger, F. M. *Environ. Sci. Technol.* **2010**, *44*, 5862.
(51) Malin, J. N.; Geiger, F. M. *J. Phys. Chem. A* **2010**, *114*, 1797.
(52) Konek, C. T.; Musorrafiti, M. J.; Al-Abadleh, H. A.; Bertin, P. A.; Nguyen, S. T.; Geiger, F. M. *J. Am. Chem. Soc.* **2004**, *126*, 11754.
(53) Wang, H.; Zhao, X.; Eisenthal, K. B. *J. Phys. Chem. B* **2000**, *104*, 8855.

(54) Subir, M.; Liu, J.; Eisenthal, K. B. *J. Phys. Chem. C* **2008**, *112*, 15809.
(55) Davis, J. A.; James, R. O.; Leckie, J. O. *J. Colloid Interface Sci.* **1978**, *63*, 480.
(56) Goldberg, S. In *Chemical Equilibrium and Reaction Models*; Leoppert, R. H., Schwab, A. P., Goldberg, S., Eds.; Soil Science Society of America Special Publication: Madison, WI, 1995; Vol. *42*.
(57) Lützenkirchen, J. *J. Colloid Interface Sci.* **1999**, *217*, 8.
(58) Urry, D. W. *What Sustains Life?: Consilient Mechanisms for Protein-Based Machines and Materials*; Springer: New York, 2006.
(59) Hiemstra, T.; Riemsdijk, W. H. V. *J. Colloid Interface Sci.* **1996**, *179*, 488.
(60) Sverjensky, D. A.; Sahai, N. *Geochim. Cosmochim. Acta* **1996**, 3773.
(61) Lützenkirchen, J. *Environ. Sci. Technol.* **1998**, *32*, 3149.
(62) Rahnemaie, R.; Hiemstra, T.; van Riemsdijk, W. H. *J. Colloid Interface Sci.* **2006**, *293*, 312.
(63) Sverjensky, D. A. *Geochim. Cosmochim. Acta* **2001**, *65*, 3643.
(64) Collins, K. D.; Neilson, G. W.; Enderby, J. E. *Biophys. Chem.* **2007**, *128*, 95.
(65) Flores, S. C.; Kherb, J.; Konelick, N.; Chen, X.; Cremer, P. S. *J. Phys. Chem. C* **2012**, *116*, 5730−5734.
(66) Liu, D.; Ma, G.; Levering, L. M.; Allen, H. C. *J. Phys. Chem. B* **2004**, *108*, 2252.
(67) Richter, L. J.; Petralli-Mallow, T. P.; Stephenson, J. C. *Opt. Lett.* **1998**, *23*, 1594.